Atmos. Chem. Phys., 10, 8601–8616, 2010
www.atmos-chem-phys.net/10/8601/2010/
doi:10.5194/acp-10-8601-2010

Atmospheric Chemistry and Physics

Novel method of generation of $Ca(HCO_3)_2$ and $CaCO_3$ aerosols and first determination of hygroscopic and cloud condensation nuclei activation properties

D. F. Zhao[1,2], A. Buchholz[2], Th. F. Mentel[2], K.-P. Müller[2], J. Borchardt[2], A. Kiendler-Scharr[2], C. Spindler[2], R. Tillmann[2], A. Trimborn[3], T. Zhu[1], and A. Wahner[2]

[1]State Key Joint Laboratory of Environmental Simulation and Pollution Control, College of Environmental Sciences and Engineering, Peking University, Beijing, 100871, China
[2]Forschungszentrum Jülich, Institut für Chemie und Dynamik der Geosphäre – 2: Troposphäre, 52425 Jülich, Germany
[3]Aerodyne Research Inc., 45 Manning Rd, Billerica, MA 01821, USA

Received: 10 March 2010 – Published in Atmos. Chem. Phys. Discuss.: 26 March 2010
Revised: 12 August 2010 – Accepted: 16 August 2010 – Published: 14 September 2010

Abstract. Atmospheric mineral aerosols contain $CaCO_3$ as a reactive component. A novel method to produce $CaCO_3$ aerosol was developed by spraying $Ca(HCO_3)_2$ solution, which was generated from a $CaCO_3$ suspension and CO_2. By aerosol mass spectrometry the freshly sprayed and dried aerosol was characterized to consist of pure $Ca(HCO_3)_2$ which under annealing in a tube furnace transformed into $CaCO_3$. Transmission Electron Microscopy demonstrated that the particles produced were spherical. The method was able to generate aerosol of sufficient concentration and proper size for the study of physiochemical properties and investigations of heterogeneous reactions of mineral aerosol.

The dried $Ca(HCO_3)_2$ particles were somewhat more hygroscopic than $CaCO_3$ particles. However, during humidification a restructuring took place and ∼2/3 of the $Ca(HCO_3)_2$ was transformed to $CaCO_3$. The mixed $Ca(HCO_3)_2/CaCO_3$(s) particles were insoluble with a growth factor of 1.03 at 95% (hygroscopicity parameter κ=0.011 ± 0.007) relative humidity. This compares to a corresponding growth factor of 1.01 for $CaCO_3$(s) (κ=0.0016 ± 0.0004). Mass spectrometric composition analysis, restructuring, and insolubility of the mixed particles suggested that solid $Ca(HCO_3)_2$(s) was observed. This would be in contrast to the current belief that $Ca(HCO_3)_2$(s) is thermodynamically instable. The CCN activity of $Ca(HCO_3)_2$(s) aerosol ($\kappa \approx 0.15$) is remarkably higher than that of $CaCO_3$ aerosol (κ=0.0019 ± 0.0007) and less than that of $Ca(NO_3)_2$. The noticeable but limited solubility of $Ca(HCO_3)_2$ of ≈ 0.01 mol/l explains limited hygroscopic growth and good CCN activity.

Experiments in the Large Jülich Aerosol Chamber indicated that $Ca(HCO_3)_2$(s) could exist for several hours under dry atmospheric conditions. However, it was likely buried in a protective layer of $CaCO_3$(s). We conclude that $Ca(HCO_3)_2$ may be formed in the atmosphere in cloud droplets of activated mineral dust by reaction of $CaCO_3$ with CO_2 and H_2O. The presence of $Ca(HCO_3)_2$ and as a consequence an enhanced CCN activity may alter the influence of mineral aerosol on global climate.

Correspondence to: Th. F. Mentel
(t.mentel@fz-juelich.de)

1 Introduction

Mineral aerosol is one of the most abundant components of aerosols in the atmosphere. It mainly arises from wind-blown soil in the deserts or semiarid areas, and also from volcanic dust, road dust and some industrial and agricultural processes. It was estimated that approximately 1000–3000 Tg of mineral aerosols are annually emitted into the atmosphere (Jonas et al., 1995). While mineral aerosol is typically considered as having a coarse mode type of distribution with particle diameters >2.5 µm, a significant number of mineral particles are also found in the fine mode with diameters in a range of 0.1–2.5 µm (Usher et al., 2003; Song et al., 2005).

On the regional scale, mineral dust has an impact on the visibility, air quality, and human health. On the global scale, it can not only influence radiative transfer by absorption and scattering of solar radiation, but also affect the cloud formation and cloud optical properties. Thus, mineral aerosols influence the global climate ultimately by direct and indirect radiative forcing. During long range transport, mineral aerosols can undergo various heterogeneous reactions and their deposition has an impact on the ocean ecosystem and the overall biogeochemical cycling. $CaCO_3$ is a common component of mineral dust, especially in East Asia and is generally regarded as the most reactive component in mineral particles (Krueger et al., 2003; Laskin et al., 2005; Sullivan et al., 2007; Usher et al., 2003). It is present at significant concentrations in both mineral aerosols (Okada et al., 2005; Zhang et al., 2003) and in surface soils (at least 5–10% by mass) of most of the major global dust sources (Claquin et al., 1999). It was found that $CaCO_3$ is among the few "volatile" components in mineral aerosols which can undergo heterogeneous reactions with atmospheric trace acids to form CO_2 (Krueger et al., 2003; Laskin et al., 2005, Santschi and Rossi, 2006). Many researchers have investigated the heterogeneous reactions of $CaCO_3$ as a surrogate for mineral dust and its impact on the physiochemical properties of mineral particles (Krueger et al., 2003; Liu et al., 2008a, b; Gibson et al., 2006). To study the physiochemical properties of mineral aerosols, the generation of surrogates of mineral aerosol components is often helpful. At present, there are two main methods to generate $CaCO_3$ aerosols, dry dispersion of solid powders (Sullivan et al., 2009a, b; Prince et al., 2007) and atomizing aqueous suspension of $CaCO_3$ powder (Gibson et al., 2006, 2007). Both methods are not easy to handle and it is difficult to generate a stable output of proper size and sufficient mass concentration. Moreover, it was observed by several groups that mineral particles generated by spray-drying of suspension are more hygroscopic than those from dry beds (Herich et al., 2009, Koehler et al., 2007, 2009, Sullivan et al., 2010). Sullivan et al. (2010) reported that for sub-100nm, wet-generated $CaCO_3$ particles the hygroscopicity parameter κ is 100 times larger than that from the dry bed generated $CaCO_3$ particles.

Compared to the method of dry dispersion of solid powders, generating aerosol by atomizing solutions does not need complex instrumentation and is easier to operate and control. However, most of the mineral dust components are characterized by very low solubility which makes atomization from solution difficult. Vlasenko et al. (2006) have used atomization of a saturated solution of $CaCO_3$ to produce $CaCO_3$ aerosol. However due to the low solubility of $CaCO_3$ in water, the number concentration of the obtained aerosol is often not high enough and the size distribution has its maximum at too small diameters considering the need of studies of physiochemical properties, such as hygroscopicity using HTDMA and CCN activation.

In order to study chemical reactions on $CaCO_3$ particles and to determine microphysical properties of the processed aerosols it would be advantageous to have at disposal an easy to handle and reproducible method for generation of $CaCO_3$ aerosol with sufficiently high particle concentration at proper size. Here we describe a novel method to generate $CaCO_3$ aerosol by atomization of solutions with enhanced amounts of dissolved $Ca(HCO_3)_2$. The basic idea is to make use of the equilibrium of $CaCO_3$ and the water-soluble form $Ca(HCO_3)_2$ in the presence of CO_2 (Reaction R1). This equilibrium is ubiquitous in natural waters when dissolved CO_2 is in contact with rocks containing $CaCO_3$. The process of dissolution of $CaCO_3$ leads e.g. to the formation of stalactites, stalagmites, columns, and other speleothems within caves when CO_2 in the water is lost and $CaCO_3$ sediment is produced (Fairchild et al., 2006; Murray, 1954).

$$CaCO_3(s) + CO_2 + H_2O \rightleftarrows Ca(HCO_3)_2(aq) \quad \text{(R1)}$$

At high CO_2 concentrations (R1) will proceed in the forward direction and cause the dissolution of the solid $CaCO_3$. On the other hand, when CO_2 is decreasing, the backward reaction will produce solid $CaCO_3$. In this study, pure CO_2 was bubbled into a slurry of $CaCO_3$ powder in order to promote the dissolution of $CaCO_3$ and formation of a $Ca(HCO_3)_2$ solution.

We will show in the following that atomizing $Ca(HCO_3)_2$ solutions, drying and annealing of the aerosol promote $CaCO_3$ formation. The aerosols produced were characterized by Scanning Mobility Particle Sizing, Aerosol Mass Spectrometry, and Transmission Electron Microscopy in order to investigate the size distribution, typical concentrations, chemical composition and morphology of the aerosol. At the same time, the aerosols before und after annealing were characterized with respect to their hygroscopicity and cloud condensation activity (CCN) activity using a Hygroscopicity Tandem Differential Mobility Analyzer (HTDMA) and a Cloud Condensation Nuclei Counter (CCNC). Here we took advantage of the different solubilities of $CaCO_3$ (0.00015 mol/l) and $Ca(HCO_3)_2$ (0.008 mol/l) at room temperature (Gmelin, 1961).

To our best knowledge this method of generating $CaCO_3$ aerosols from a CO_2 containing solution of $Ca(HCO_3)_2$ has not been described before. Moreover, not much attention has been paid to the possible importance of $Ca(HCO_3)_2$ which could be formed in the atmosphere in cloud droplets of activated mineral dust containing $CaCO_3$ by reaction with CO_2 and H_2O.

2 Experimental

2.1 Preparation of $Ca(HCO_3)_2$ solution

$Ca(HCO_3)_2$ solutions were prepared at room temperature ($\sim$22°C) by bubbling CO_2 (Praxair Industriegase GmbH&Co. KG, purity 99.995%) at a gauge pressure of

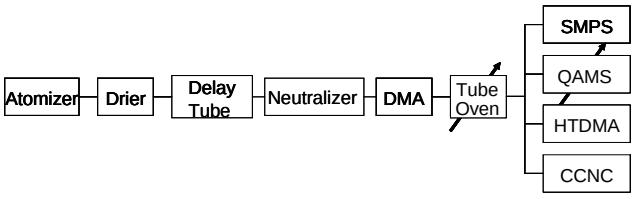

Fig. 1. Schematics of experimental set up (details see text).

20 mbar from the cylinder into 1 L of water (Milli-Q, 18.2 MΩcm, TOC <5 ppb) containing 2 g $CaCO_3$ powder (pro analysis, ≥99%, Merck). During CO_2 bubbling the slurry was stirred using a magnetic stirrer to promote the suspension of solid $CaCO_3$ in the water. After bubbling, the slurry was allowed to settle for 5 min and the supernatant clear $Ca(HCO_3)_2$ solution was decanted.

In order to characterize the reproducibility of the method and the stability of the solution for aerosol generation, different CO_2 bubbling durations were applied and the solutions were atomized over longer periods. The aerosol was dried and the number density and the count median of the size distribution were determined. It was found that stirring the slurry helped to reach the equilibrium faster.

In order to avoid introducing possible contaminants to the aerosol, careful measures in preparing solutions and subsequent spraying were taken into account. This included using high purity agents, gas, water and careful cleaning of bottles, tubes and atomizer to our best effort.

2.2 Generation of $CaCO_3$ particles

The $Ca(HCO_3)_2$ solution was sprayed by a constant output atomizer (TSI, Model 3076) using synthetic air (Linde LiPur 6.0, purity 99.9999%). The generated aerosol passed through a diffusion drying tube filled with silica gel (final RH < 5%) and a delay tube to equilibrate charges (Dinar et al., 2006), as shown in Fig. 1. The number size distribution of the resulting aerosol was measured by an SMPS system (TSI, DMA 3071, CPC 3022A).

At room temperature $Ca(HCO_3)_2$ should be thermodynamically unstable as a solid and only exist in solution as Ca^{2+} and HCO_3^- (Keiser and Leavitt, 1908; Miller, 1952; House, 1981). Upon drying, it is supposed to convert to $CaCO_3$ very easily at room temperature. However, as shown in the following, the aerosols generated from spraying $Ca(HCO_3)_2$ solutions still contained a significant amount of $Ca(HCO_3)_2$ after drying. We therefore used a tube furnace at 300 °C in order to promote the transformation of $Ca(HCO_3)_2$ to $CaCO_3$ aerosol. The temperature of the tube furnace was set to 300 °C because at this temperature $Ca(HCO_3)_2$ should already decompose to form $CaCO_3$ (Reaction R2) while $CaCO_3$ is still stable (Keiser and Leavitt, 1908; Sanders and Gallagher, 2002).

$$Ca(HCO_3)_2(s) \rightarrow CaCO_3(s) + CO_2 + H_2O \quad \text{(R2)}$$

The whole setup as used is shown in Fig. 1. After the delay tube the aerosol was neutralized (TSI, 3077) and size selected by a DMA (TSI, DMA 3071). The size-selected aerosol passed the tube furnace which was either at room temperature or set to 300 °C. After the furnace the aerosol flow was split and directed to the different instruments. A Quadrupole Aerosol Mass Spectrometer (Q-AMS, Aerodyne Research Inc., Jayne et al., 2000) was used to characterize the composition of aerosols. HTDMA and CCNC (Droplet Measurement Technologies, DMT-100) were used to investigate the hygroscopicity and CCN activity.

2.3 Characterization of chemical composition and morphology of the aerosol

Chemical characterization of the aerosols was provided by the Q-AMS by measuring H_2O and CO_2 evaporating off the particles. In the Q-AMS a focused particle beam is generated by an aerodynamic lens. This beam impacts on the heated surface of a vaporizer which is located in the ionization region of a Quadrupole Mass Spectrometer. The ionization of the vapor is achieved by electron impact ionization with electrons of 70 eV. The Q-AMS is routinely operated in two alternating modes. In the so called MS-mode, the size integrated particle composition is measured. In the so called pToF-mode (particle time of flight mode), the size resolved composition is observed for a set of selected mass to charge ratios (*m/z*). From the combination of the MS-mode and the pToF-mode data, which were measured alternating with 5 min time resolution, the size dependent chemical composition over the accessible particle size range is retrieved. Details of the mode of operation of the Q-AMS are described in Jayne et al. (2000).

Water, mainly detected on the *m/z* 18 (H_2O^+), and CO_2, mainly detected at *m/z* 44 (CO_2^+), served to determine the bicarbonate and carbonate content. Water and CO_2 were quantified from the MS spectra as described in Allan et al. (2004). The relative ionization efficiency (RIE) of CO_2 was set to 1.4, for H_2O we applied an RIE of 2 which was recently determined by Mensah et al. (2010). Blank measurements with a HEPA filter in line were conducted before each experiment and the *m/z* 18 and *m/z* 44 were lower than 0.3 µg m^{-3} and 0.04 µg m^{-3}, respectively. During experiments the value of *m/z* 18 and *m/z* 44 for the aerosols was up to tens of µg m^{-3}.

The detection and discrimination of $Ca(HCO_3)_2$ and $CaCO_3$ by the Q-AMS was accomplished by tuning the temperature of the vaporizer to 300 °C or 900 °C according to the thermal properties of $Ca(HCO_3)_2$ and $CaCO_3$. When the temperature of the vaporizer was set to 300 °C, $Ca(HCO_3)_2$ in the aerosol decomposed at the vaporizer according to (Reaction R2) and was detected in the form of CO_2 and H_2O. When the temperature of the vaporizer was set to 900 °C, both $Ca(HCO_3)_2$ and $CaCO_3$ are decomposed Reactions (R3, R4), whereat $Ca(HCO_3)_2$ should deliver two CO_2 and one

H_2O per formula unit, whereas $CaCO_3$ is supposed to evaporate only one CO_2 per formula unit.

$$Ca(HCO_3)_2(s) \rightarrow CaO(s) + 2CO_2 + H_2O \quad \text{(R3)}$$

$$CaCO_3(s) \rightarrow CaO(s) + CO_2 \quad \text{(R4)}$$

By interplay of the annealing temperature of the tube furnace and the temperature of the vaporizer of the Q-AMS the content of $CaCO_3$ and $Ca(HCO_3)_2$ in the aerosol was determined according to Reactions (R2–R4). (*Defacto* we bypassed the tube furnace for the measurements at room temperature, i.e. we measured before and after annealing in the tube furnace.). Because of the gas-phase suppression factor of 10^7 of the Q-AMS, the contribution of H_2O(g) and CO_2(g) evaporating from $Ca(HCO_3)_2$ in the furnace on *m/z* 18 and *m/z* 44 is negligible.

The particle mass distribution as function of the vacuum aerodynamic diameter was observed in the pToF mode of the Q-AMS. By comparing the modal positions of this particle mass distribution and of the particle volume size distribution calculated from the number size distribution measured by the SMPS, the effective particle density was obtained (DeCarlo et al., 2004).

In order to get information about the morphology of the particles, aerosol was sampled before and after annealing on a copper grid using a home-built aerosol sampling device (Marquardt et al., 1992) and characterized by Transmission Electron Microscopy (TEM). In the sampling device, a high voltage was applied and aerosol particles were deposited in the electric field onto the copper grid which was positioned in the centre of the gas flow.

2.4 HTDMA operation

The hygroscopic growth of the particles was measured with a home built HTDMA (Buchholz, 2007). With the first DMA (TSI 3071) particles were selected from the dried polydisperse aerosol with an electromobility diameter of 150 nm. The second DMA (TSI Model 3071) was operated in a scan mode and the particles were detected by a condensation particle counter (TSI CPC 3022A). Both DMA were operated with 0.3 lpm aerosol sample flow and 3 lpm sheath air flow.

The size selected aerosol and the sheath air of the second DMA were humidified at a temperature of 27 °C to almost the same relative humidity (RH) with the sheath air being at slightly higher RH. The second DMA is placed in an insulated box and cooled to 20 °C. Before entering the second DMA both aerosol and sheath air were cooled down to the same temperature and thus the RH increased to its final value. The particles remained for approximately 20 s in contact with the final humidity before they enter the SMPS which was operated with sheath air of the same humidity. To determine the RH inside the second DMA the absolute humidity was calculated from RH and T data of two Vaisala HMP235 sensors before and after the insulated area. In addition the temperatures of the air flows inside the insulated area were measured with PT100 sensors directly before or after they entered or left the DMA. For calibration ammonium sulfate aerosol was used.

2.5 CCN operation and evaluation

To determine the CCN activity, the polydisperse aerosol was size selected by scanning a DMA between 10 and 450 nm. For each size bin the total number of particles (CN) was detected with an ultrafine water CPC (UWCPC, TSI 3786) and the number of activated particles (CCN) at different supersaturations (SS) was measured in parallel with a continuous flow CCNC (Droplet Measurement Technologies, DMT-100). The ratio of CCN to CN is called activated fraction. Since a DMA selects electromobility diameters, multiple charged particles with accordingly larger diameters entered the CCN counter, too. The fraction of these particles contributes to activation at the small diameters. For a correct interpretation of activation diameters the fraction of multiple charged particles was calculated according to a natural charge distribution (Wiedensohler, 1988). The activated fraction was then determined for each charge class separately and an error function was fitted to the data. The dry activation diameter (or critical dry diameter, D_{crit}) is the turning point of this distribution.

For each SS at least three scans were performed and the resulting D_{crit} were averaged. For calibration D_{crit} of ammonium sulfate was measured for five different SS.

2.6 Aerosol chamber experiments

The long term behavior of the carbonate aerosols was studied in the Jülich Large Aerosol Chamber (Mentel et al., 1996). Before any experiment with $Ca(HCO_3)_2/CaCO_3$ we determined the background concentration of HNO_3 in the chamber by sampling a continuous air stream of 1 lpm through a stripping solution (1% $CaCl_2$ w/w) in a washing bottle. The stripping solution was backed-up by a second washing bottle with the same solution. The nitrate content of the stripping and the backup solution were analyzed by ion chromatography. The background HNO_3 concentration was estimated to be 1.1 ± 0.5 ppb at a RH of 30%.

In order to generate the aerosols the solution containing $Ca(HCO_3)_2$ was prepared as described above and sprayed by ten two-fluid nozzles against the walls of a small prechamber to impact larger droplets (Wahner et al., 1998). The generation air stream of 140 lpm served to flush the submicron portion of the $Ca(HCO_3)_2$(aq) into the large chamber. This air stream is saturated with water vapor and the aerosol is conditioned in the large chamber by mixing with the chamber air. Nevertheless, the RH rises in the large chamber by the generation air stream; typically a flushing for 20 min raised the RH by less than 2% at 290 K.

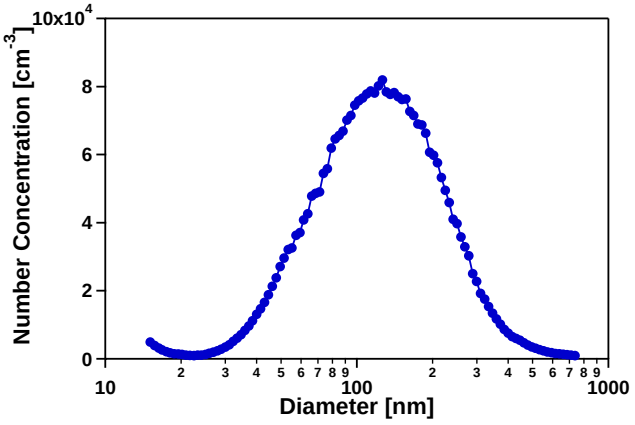

Fig. 2. Typical dry size distribution of aerosols generated by atomizing the $Ca(HCO_3)_2$ solutions with a TSI3076 constant output nebulizer. The aerosols were dried to RH <5% in a diffusion drier using Silica gel as desiccant.

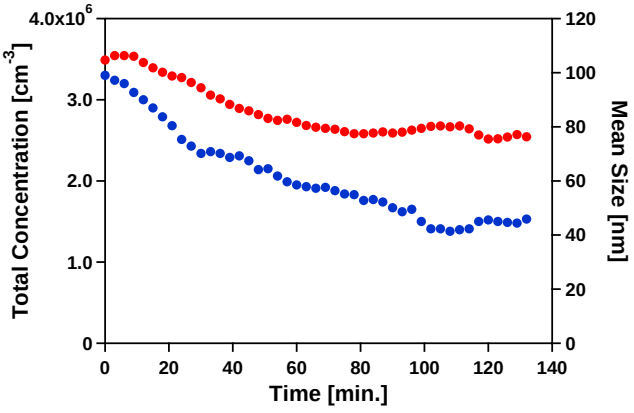

Fig. 3. Change with spraying time of the total number concentration (blue, left axis) and the mean size (red, right axis) of dry aerosols generated by atomizing $Ca(HCO_3)_2$ solution.

We performed three types of experiments. In the first experiment the large aerosol chamber was flushed for several hours with dry synthetic air (Linde LiPur 6.0, purity 99.9999%) without CO_2 (final RH < 3%) and only the aerosol was added in one step. The experiment lasted 36 h and was repeated once wherein the aerosol was monitored for 24 h. In the second experiment the chamber was flushed with particle free outside air leading to a RH of 40%. The outside air contained about 400 ppm CO_2. The aerosol was added to the chamber in two steps with 3 h in between. In the third experiment the chamber was flushed with dry synthetic air without CO_2, but then humidified by evaporating water (MilliQ) to approximately 40% RH. Initially 370 ppb NO, 100 ppb NO_2, and 370 ppb O_3 were filled into the chamber and after 2 h the aerosol was added. In all cases we measured the size distribution, CCN activation, hygroscopic growth, and the ratio $Ca(HCO_3)_2/CaCO_3$.

3 Results and discussions

3.1 Size distribution and stability of aerosol generation

Different CO_2 bubbling durations were applied at room temperature to determine the time required for formation of sufficient $Ca(HCO_3)_2$ and for the dissolving process to reach equilibrium. For this, the total number concentration N_{tot} of the dried aerosol generated from the respective solutions served as a measure. N_{tot} increased fast with increasing bubbling duration but leveled off after >2 h of bubbling. After 1 h of CO_2 treatment the aerosol number concentration has reached 80% of the maximum concentration.

To ensure equilibrium, CO_2 was bubbled through the stirred, aqueous $CaCO_3$ suspension for 3 h to prepare the $Ca(HCO_3)_2$ solutions. A typical size distribution of aerosol generated from $Ca(HCO_3)_2$ solution is shown in Fig. 2. The number concentration peaked at ∼120 nm with a geometric standard deviation of ∼1.8.

The stability of the solution was tested by continuous spraying of the same solution over a longer period. N_{tot} and the count median diameter of the number size distribution served as a measure of stability (Fig. 3). First the number concentration of the aerosol decreased with spraying time and then leveled off after 100 min. Meanwhile, the median size of aerosol decreased gradually from 120 nm to ∼80 nm over 2 h. During spraying of the solution a white deposit was formed in the storage bottle and the connecting tubes. This can be explained, since the solution was sprayed with synthetic air, free of CO_2. The solution lost excess CO_2 and solid $CaCO_3$ was formed. As $CaCO_3$ deposits from the solution, the concentration of $Ca(HCO_3)_2$ aerosol was decreased resulting in a decrease of both the number concentration and median size of the particles.

3.2 Particle density and morphology

The particles were size selected at an electromobility diameter of 150 nm (Fig. 4). The peaks at 150 nm, 233 nm, and 300 nm corresponded to the single, double and triple charged particles. After passing the tube furnace at 300 °C, the size of the particles decreased to 138 nm, 216 nm, and 279 nm, respectively.

A corresponding decrease of the vacuum aerodynamic size was observed in the pToF mode of the Q-AMS as can be recognized in Fig. 5. From the mode positions of the mass size distribution ($D_{max\ va}$) measured by Q-AMS and of the volume size distribution ($D_{max\ em}$) derived from the SMPS data, an effective density (ρ_{eff}) was obtained according to

$$\rho_{eff} = \frac{D_{max\ va}}{D_{max\ em}}. \quad (1)$$

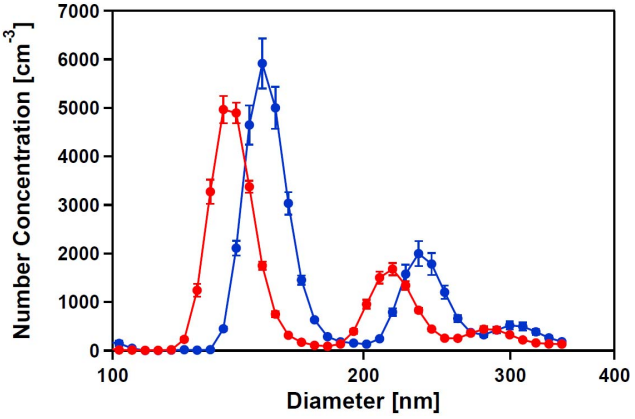

Fig. 4. Size distribution of neutralized, dry particles, electromobility selected at 150 nm, *before* (blue) and *after* (red) annealing at 300 °C in the tube furnace. The particles were generated by atomizing a $Ca(HCO_3)_2$ solution.

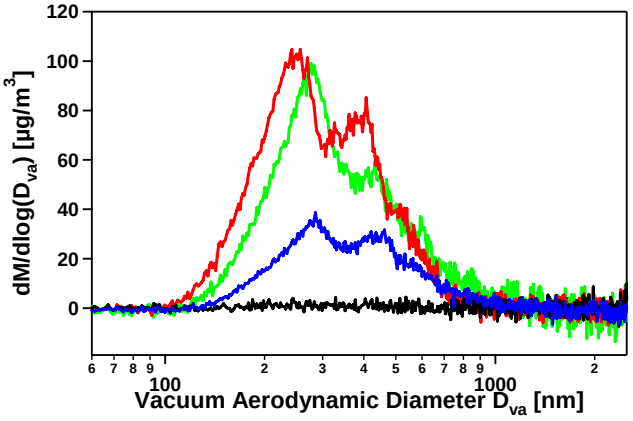

Fig. 5. Mass size distributions derived from the CO_2^+ signal in the pToF mode of the Q-AMS. Blue: aerosol *before annealing*, AMS vaporizer at 300 °C (case 1), black: aerosol *after annealing* at 300 °C, Q-AMS vaporizer at 300 °C (case 2), green: aerosol *before annealing*, Q-AMS vaporizer 900 °C (case 3), , red: aerosol *after annealing* at 300 °C, Q-AMS vaporizer 900 °C (case 4).

The respective ρ_{eff} were 1.83 ± 0.1 g/cm^3 before the furnace and 1.79 ± 0.1 g/cm^3 after the furnace, thus the same within the errors. The effective density of the generated aerosol is lower than the bulk density of calcite or aragonite of 2.71 and 2.83 g/cm^3, respectively, which implies that it is not compact crystalline $CaCO_3$.

TEM was used to obtain images of the particles as shown in Fig. 6. Aerosol particles generated from the $Ca(HCO_3)_2$ solution were spherical with a heterogeneous distribution of round structures, some of which look like hollow pits on the surface or spherical structures inside. After annealing in the furnace, these round structures became much finer and evenly distributed on the surface implying that the particles restructured during the annealing process.

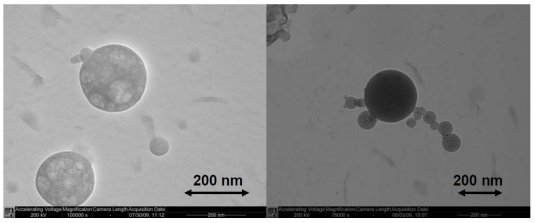

Fig. 6. TEM images of aerosol particles before **(a)** and after **(b)** annealing at 300 °C in the tube furnace. The aerosol particles were generated by atomizing the $Ca(HCO_3)_2$ solutions and dried before deposition on the TEM grids.

3.3 Particle chemical composition

The composition of the aerosols was retrieved from the Q-AMS data. Remember, that we alternated the combination of two heated devices: the tube *furnace* at 300° to anneal the aerosols before the Q-AMS measurement and the *vaporizer* of the Q-AMS to flash-evaporate the particles for detection. (We will strictly use these notations *furnace* and *vaporizer* in the following.) We compared the following four combinations (see also Table 1): Q-AMS vaporizer at 300 °C probing *before* (case 1) and *after* (case 2) tube furnace at 300 °C, Q-AMS vaporizer at 900 °C probing *before* (case 3) and *after* (case 4) the tube furnace at 300 °C.

The Q-AMS data were converted from mass to mole numbers and normalized to the Ca content retrieved from the respective SMPS data as follows. To get the aerosol mass concentrations, the volume size distributions were integrated from 60 nm–700 nm and multiplied with ρ_{eff}. Dividing by the molecular weights of $Ca(HCO_3)_2$ and $CaCO_3$ gives the number of moles of the salts thus of Ca per unit volume of air before and after the furnace respectively. This is an anticipation of the following results, thus a working hypothesis at this stage. The normalization to Ca as a conserved quantity is very helpful but not crucial for the following analysis. (The normalization to SMPS data compensated for day to day variations in the aerosol concentrations. As will be shown below an analysis based on normalization to the particle mass instead of Ca led to the same results.) Of course it would have been easier to normalize to a Q-AMS internal quantity. However, neither Ca nor total mass of the carbonates can be measured quantitatively by the Q-AMS since the CaO resulting from Reactions (R3 and R4) is not flash-evaporating completely at Q-AMS vaporizer temperatures of 300 °C or 900 °C. However we can also benefit from the normalization to SMPS based Ca since it allows for testing the collection efficiency (CE) of the Q-AMS. Note already here, that the CE was ∼50% in case 1 and 3. The CE was close to 100% in case 4 and cannot be determined for case 2. This will be discussed in more detail below.

Table 1. Species detected at different temperatures T of tube furnace and Q-AMS vaporizer

Case No.	$T_{furnace}$	$T_{vaporizer}$	Species detected	n_{CO_2}	n_{H_2O}
1	22 °C (bypass)	300 °C	$Ca(HCO_3)_2$ before furnace (R2)	x	$x+z$
2	300 °C	300 °C	$Ca(HCO_3)_2$ after furnace (R2)	no	no
3	22 °C (bypass)	900 °C	$Ca(HCO_3)_2$+$CaCO_3$ before furnace (R3, R4)	$2x+y$	$x+z$
4	300 °C	900 °C	$Ca(HCO_3)_2$ + $CaCO_3$ after furnace(R3, R4)	$x+y$	no

n_{CO_2} and n_{H_2O}: detectable mole numbers of CO_2 and H_2O per formula unit of $x Ca(HCO_3)_2 \cdot y CaCO_3 \cdot z H_2O$

The molar ratios CO_2/Ca, H_2O/Ca based on Q-AMS/SMPS and the molar ratio of H_2O to CO_2 based on the Q-AMS data only are shown in Fig. 7a, b and c, respectively. The error bar represents the standard deviation of repeated measurements. As mentioned above, at the Q-AMS vaporizer temperature of 300 °C we expect to detect $Ca(HCO_3)_2$ by one CO_2 and one H_2O by the Q-AMS, because of the incomplete thermal decomposition (R2). At the vaporizer temperature of 900 °C thermal decomposition (R3) is complete and two CO_2 and one H_2O should be detected. $CaCO_3$ is not detected at 300 °C but at 900 °C where one CO_2 is formed.

For the aerosol *before* annealing significant amounts of CO_2 were detected at 300 °C Q-AMS vaporizer temperature (case 1, Fig. 7a). The measured amount doubled when the vaporizer was turned to 900 °C (case 3, Fig. 7a). The detected amount of H_2O was the same for both vaporizer temperatures (Fig. 7b). The molar ratio of H_2O to CO_2 was close to 1 at 300 °C and close to 0.5 for 900 °C, respectively (Fig. 7c). This means that before annealing the aerosol consisted of nearly pure $Ca(HCO_3)_2$ with no additional water in the particles and that all $Ca(HCO_3)_2$ was destroyed on the vaporizer of the Q-AMS at 300 °C. Nevertheless, the ratios CO_2/Ca and H_2O/Ca in cases 1 and 3 are only half as large as expected from stoichiometry indicating a reduced CE of the Q-AMS.

For particles that were annealed in the tube furnace to 300 °C neither CO_2 nor H_2O was detected at 300 °C vaporizer temperature (case 2), because all thermally available CO_2 and H_2O were already driven out in the tube furnace (Fig. 7a and b). This also means that after annealing in the furnace, the aerosol consisted of nearly pure $CaCO_3$. In case 2 small values near the detection level were leading to the large errors bars in Fig. 7c. At 900° vaporizer temperature (case 4) we observed only a very small amount of H_2O, but a large signal of CO_2 (Fig. 7b and 7a).

If the particles consisted of pure $Ca(HCO_3)_2$ before annealing and of pure $CaCO_3$ thereafter, one CO_2 is lost by conversion of $Ca(HCO_3)_2$ to $CaCO_3$ (Reaction R2) in the tube furnace. Therefore we should observe for Q-AMS vaporizer temperatures of 900 °C only half of the CO_2 after annealing. However, comparing the cases 3 and 4 the CO_2 signals before and after annealing have the same magnitude. This cannot be due to incomplete conversion of $Ca(HCO_3)_2$ to $CaCO_3$ because only little water is observed in case 4. Also large shape factor effects can be excluded since the particles kept their overall spherical shape after passing the furnace (Fig. 6). The *observed as expected* mole ratios of H_2O/CO_2 in cases 1 and 3 (Fig. 7c) and *the observed as expected* doubling of the CO_2 amount going from case 1 to case 3 excludes simple effects of the different vaporizer temperatures.

The observed CO_2/Ca ratios (Fig. 7a) and H_2O/Ca ratios (Fig. 7b) indicate that the CE of the Q-AMS must be differed between the cases. The data are consistent with a CE of about 50% in cases 1 and 3 and near 100% in case 4. This is dissatisfying. Collection efficiencies for solid particles below 100% have been observed before. This is explained by solid particles bouncing off the vaporizer surface before full evaporation (Matthew et al., 2008). Note in Fig. 5 that our mass distributions were within the transmission window of 60–600 nm, and the little tailing at large diameters into the fall off range of the aerodynamic lens cannot cause effects of a factor of two. Unfortunately, we intrinsically cannot observe a signal in case 2. This prevents testing if annealing of the particles at 300 °C and conversion from $Ca(HCO_3)_2$ to $CaCO_3$ has led to higher CE. However, higher CE for tempered solid particles compared to freshly dried particles seems to be somewhat anti-intuitive. We repeated the experiments with virtually the same results, i.e. enhanced CO_2 and CE in case 4 is not a singular artifact. It remains unexplained for the moment, but adds only little uncertainty to our findings. All other evidence supported that we produced pure $Ca(HCO_3)_2$ aerosol by spraying the solution and drying the aerosol to RH < 5% and that we were able to convert it to $CaCO_3$ by annealing it at 300 °C. Moreover, because of the H_2O/CO_2 stoichiometry in cases 1 and 3 (Fig. 7c) and the absence of excess water (Fig. 7b, c), we can rule out inclusions of aqueous phase and the formation of metastable $CaCO_3$ hydrates as described e.g. by Brecevic and Kralj (2007).

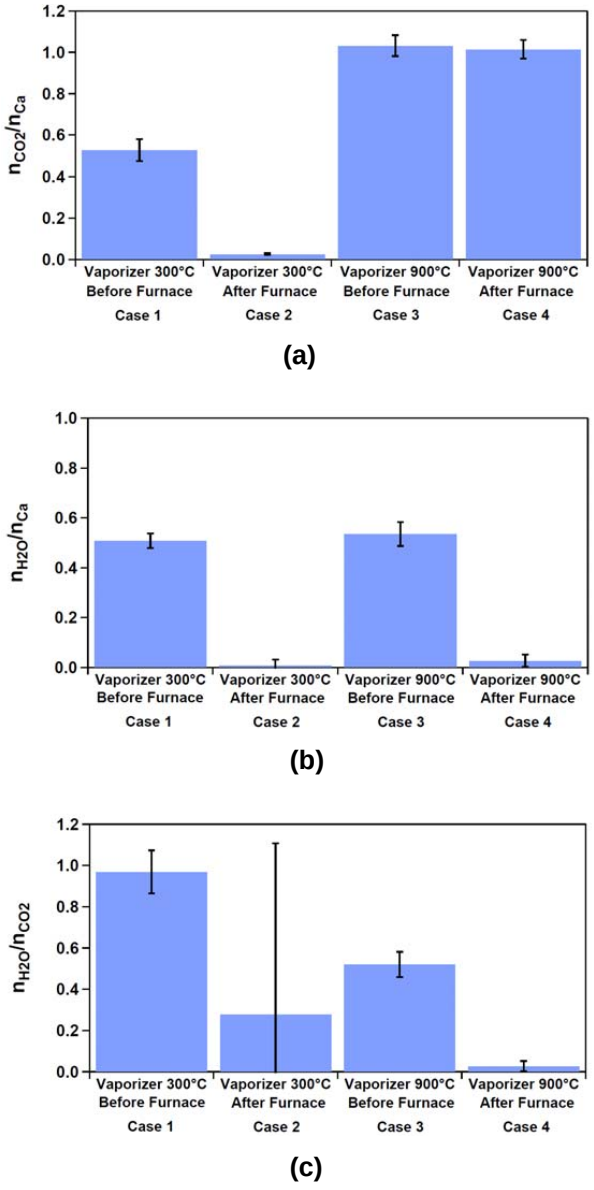

Fig. 7. Mole numbers of CO_2 (n_{CO_2}, **a**), H_2O (n_{H_2O}, **b**) detected at different temperatures of the Q-AMS vaporizer before and after annealing in the tube furnace. The mole numbers of CO_2 and H_2O were derived by AMS and in (a) and (b) normalized to the Ca mole number (n_{Ca}) derived from SMPS measurements. The mole ratio n_{H_2O}/n_{CO_2} **(c)** is based on AMS data only. Error bars are the standard deviations from repeated AMS measurements, respective the accordingly propagated errors in (c).

The general composition of the generated carbonate aerosols can be written as $xCa(HCO_3)_2 \cdot yCaCO_3 \cdot zH_2O$. The combination of furnace temperature and the Q-AMS vaporizer temperature and the corresponding species detected are listed in Table 1. If the total calcium salt is normalized to unity, then y equals $1-x$. The parameters x, y, z then can be obtained from the Eqs. (2–7):

Table 2. Composition of aerosol before and after the furnace.

	$T_{furnace}$ [°C]	x	y	z
Before furnace	22	1.05	−0.05	−0.032
After furnace	300	0.027	0.97	–

formula unit: $xCa(HCO_3)_2 \cdot yCaCO_3 \cdot zH_2O$

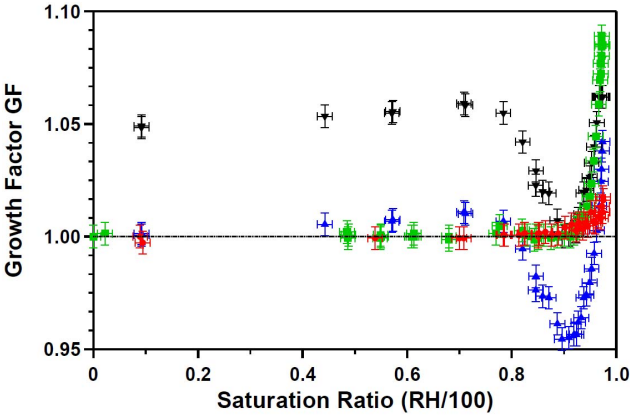

Fig. 8. Humidograms of calcium carbonate aerosols size selected at an electromobility diameter of 150 nm. $CaCO_3$ (red dots), $Ca(HCO_3)_2$ (blue triangles), $Ca(HCO_3)_2$ normalized to the minimum diameter at RH 89.5% (black triangles), and $Ca(HCO_3)_2$ pre-conditioned at 100% RH and dried before size selection (green squares). Measurement errors: saturation ratio ±0.014, GF ±0.005.

$$\frac{n_{nCO_2}(900°)}{n_{nCO_2}(300°)} = \frac{1+x}{x} \quad (2)$$

$$r_1 = \frac{n_{nCO_2}(900°)}{n_{nCO_2}(300°)} \quad (3)$$

$$x = \frac{1}{r_1 - 1} \quad (4)$$

$$\frac{n_{nH_2O}(300°)}{n_{nCO_2}(300°)} = \frac{x+z}{x} \quad (5)$$

$$r_2 = \frac{n_{nH_2O}(300°)}{n_{nCO_2}(300°)} \quad (6)$$

$$z = (r_2 - 1) \cdot x \quad (7)$$

Herein $n_{nCO_2}(900°)$ is the mole number of CO_2 in the aerosol *normalized* to the aerosol *mass* concentration before annealing (22 °C) detected at 900 °C in the AMS and n_{nH_2O} (300 °) and n_{nCO_2} (300 °) are the mole numbers of H_2O and CO_2 normalized in the same way but detected at 300 °C in the AMS.

The composition of the aerosol before and after annealing was determined this way and is shown in Table 2. For the aerosol before the furnace, x was near unity and y and z were

Table 3. Measured and calculated normalized mass $m_n(CO_2)$ and $m_n(H_2O)$.

Case No	$T_{VAPORIZER}$	measured $m_n(CO_{2)}$	calc. $m_n(CO_2)$	meas. /calc.	measured $m_n(H_2O)$	calc. $m_n(H_2O)$	meas. /calc.
1	300 °C before furnace	0.146	0.272	0.53	0.056	0.111	0.51
2	300 °C after furnace	0.012	0	–	0.001	0	–
3	900 °C before furnace	0.280	0.543	0.52	0.059	0.111	0.54
4	900 °C after furnace	0.446	0.440	1.01	0.005	0	–

The measured mass concentrations of CO_2 and H_2O were normalized to the aerosol mass concentration derived from SMPS volume and effective density ρ_{eff}. Calc. refers to the compositions obtained in Table 2.

zero within the error limits (the value of x should be less than or equal to 1 and x, y, z should be positive) which means almost the whole particle consisted of $Ca(HCO_3)_2$. The ratio of z to x was near zero indicating there is no additional water. In contrast, after the furnace, the particle consists of almost pure $CaCO_3$ with very little $Ca(HCO_3)_2$ being left. This is consistent with the analysis discussed above.

From the composition of the aerosol in Table 2, the mass concentration of CO_2, H_2O normalized to the aerosol mass concentration were calculated as a theoretical value and compared with the measured value (Table 3). The ratio of measured to calculated concentrations gives an estimate of CE supporting the above mentioned values of ∼50% in cases 1 and 3 and of 100% in case 4.

Based on the analysis of the composition of the aerosol above, we will refer to the dried aerosol before annealing in the furnace as $Ca(HCO_3)_2$ aerosol and to the aerosol after annealing as $CaCO_3$ aerosol in the following. We hypothesize that the $Ca(HCO_3)_2$ particles were solid, although it is known that solid $Ca(HCO_3)_2$ is thermodynamically instable at ambient conditions. The $CaCO_3$ particles were pure solids within the errors of the analysis but may have contained traces of $Ca(HCO_3)$.

3.4 Hygroscopicity of the aerosol

The humidograms of the laboratory generated aerosols are shown in Fig. 8. $CaCO_3$(s) aerosol (red dots) took up only very little water at very high RH and deliquescence was not observed up to RH of 97.4(±1.4)%. We calculated hygroscopicity parameters κ according to the one parameter representation of the Köhler equation proposed by Petters and Kreidenweis (2007). By averaging κ in the range 97–97.4% RH we obtained a κ_{GFCO3} of 0.0016 ± 0.0004.

Dried $Ca(HCO_3)_2$ aerosols (blue triangles) showed a different growth behavior. Up to RH of 71(±1.4)% the particle diameter increased by 1%. Between 71% and 78% the growth factor (GF) decreased and reached a minimum of 0.95 at RH 89.5(±1.4)%. Thereafter the particles grew continuously with increasing RH without showing a distinct deliquescence point. Condensation of small amounts of water (GF = 1.01 at 71% RH) obviously caused shrinking of the particles probably due to some water aided restructuring of the particles (compare the TEM image in Fig. 6a, which indicates inhomogeneities on or in the particles.). Shape effects can be excluded since the dried particles were already spherical.

To test the effect of wetting the dry $Ca(HCO_3)_2$ particles, the aerosol was humidified to almost 100% and then *dried again* before entering the instruments. After the preconditioning (pc) the minimum in the growth curve disappeared and the particles did not grow until ca. 92% (Fig. 8, green squares). The uptake of water already occurred at lower RH and was higher than for $CaCO_3$. No distinct deliquescence point was observed. We calculated κ in the range 97–97.5%RH and obtained an average κ_{GFpc} of 0.011 ± 0.007 for the pre-conditioned $Ca(HCO_3)_2$ aerosol.

When the growth curve of the non-conditioned (nc), dry $Ca(HCO_3)_2$ aerosol was shifted using the diameter of the minimum at RH 89.5% as reference diameter (Fig. 8, black triangles), the high humidity branches at RH > 93% for the particles with and without pre-conditioning agree within the errors, thus should have the same composition and morphology. We calculated an average $\kappa_{GFnc} = 0.008 \pm 0.003$ between 97–97.5% RH for the non-conditioned $Ca(HCO_3)_2$ aerosol from the shifted humidogram. This is smaller than κ_{GFpc} but still agrees within the uncertainties.

The Q-AMS analysis showed that the pre-conditioned and then dried again particles consisted of ∼67% $CaCO_3$ and ∼33% $Ca(HCO_3)_2$. The conditioning process can be imagined as dissolving some bicarbonate in the water layer, where it decays and CO_2 evaporates. This is the same process as occurring in weathering of carbonate rocks. In comparison to the pure $CaCO_3$, the presence of $Ca(HCO_3)_2$ increased the growth factors and thus shifted the growth curve to lower RH.

Table 4. Critical parameter of CCN activation observed in the laboratory study.

SS_{crit} [%]	$CaCO_3$ D_{crit} [nm]	$Ca(HCO_3)_2$ D_{crit} [nm]	$CaCO_3/Ca(HCO_3)_2$ (67%/33%) D_{crit} [nm]
0.10		256	210
0.15		174	162
0.20		139	127
0.24		118	110
0.29		102	100
0.48		72	74
0.57	239		67
0.67	202		60
0.76	173		55
0.85	152		
0.95	136	46	48

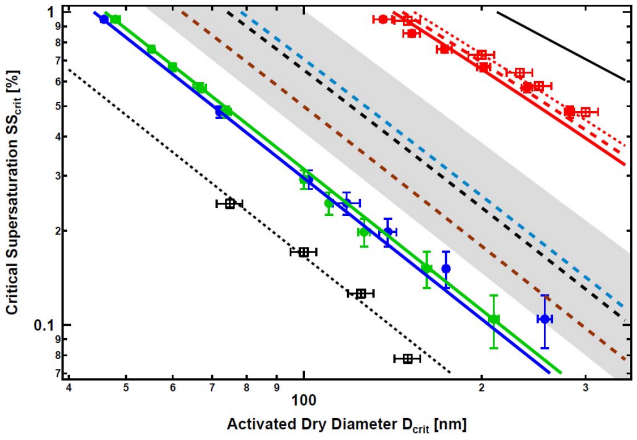

Fig. 9. Critical supersaturation as function of the activated dry diameter: $CaCO_3$ (red dots), $Ca(HCO_3)_2$(s) (blue dots), and mixed $CaCO_3/Ca(HCO_3)_2$(s) (green dots). Red, blue and green solid lines represent one parameter Köhler calculations assuming κ=0.0019, $\kappa = 0.16$ and $\kappa = 0.14$, respectively. For comparison results of Sullivan et al. (2009b) are given for $CaCO_3$ (red open squares) with $\kappa = 0.0011$ (red dotted line) and $Ca(NO_3)_2$ (black open squares) with $\kappa = 0.051$ (black dotted line). The shaded area comprises the range of expectation for activation of atmospheric mineral dust according to Koehler et al. (2009). The dashed lines are one parameter Köhler representations of their suggested median κ of 0.03 (black), Arizona Test Dust ($\kappa = 0.025$, blue) and Saharian Dust ($\kappa = 0.054$, brown) (Koehler et al., 2009). The red dashed line represents the average κ_{CO_3} based on the combination of this study and of Sullivan et al. (2009b).

The moderate growth at RH < 71 % of the non-conditioned, dried $Ca(HCO_3)_2$ particles and the restructuring supports our hypothesis that these particles were solid. It must be a metastable solid phase; the sudden evaporation of water in the drying process seems to hinder the formation of thermodynamically stable $CaCO_3$. Also the pre-conditioned, mixed particles did not show growth at RH < 92% although they contained 33% $Ca(HCO_3)_2$. This indicates that these mixed particles were also solid.

$Ca(HCO_3)_2$(s) seemed to become unstable at RH > 71% even on the short time scales of the HTDMA measurement. It is likely that with increasing humidity the composition of the particles shifted towards ~67% $CaCO_3$ and ~33% $Ca(HCO_3)_2$, as indicated by the similarity of κ_{GFpc} and κ_{GFnc}. Because of this instability the hygroscopic growth behavior of pure $Ca(HCO_3)_2$ could not be determined. However, it should be much more hygroscopic than $CaCO_3$(s) and the $CaCO_3/Ca(HCO_3)_2$(s) mixed salt as indicated by the GF of 1.01 at RH 71% (see Fig. 8, blue triangles).

We can estimate κ_{HCO3} for $Ca(HCO_3)_2$ under the assumptions of constant composition of the mixed $CaCO_3/Ca(HCO_3)_2$(s) aerosol over duration of the succeeding humidogram and a homogenous distribution of $Ca(HCO_3)_2$ and $CaCO_3$ within the particles, thus equal availability for the condensing water:

$$\kappa_{GFpc} = f_{CO_3} \cdot \kappa_{CO_3} + f_{HCO_3} \cdot \kappa_{HCO_3}$$
$$\kappa_{HCO_3} = \frac{\kappa_{GFpc} - f_{CO_3} \cdot \kappa_{CO_3}}{f_{HCO_3}} \quad (8)$$

Herein f_x are the volume fractions of $CaCO_3$ and $Ca(HCO_3)_2$, respectively. For simplicity we assume that $CaCO_3$ and $Ca(HCO_3)_2$ feature the same density, in agreement with the equal ρ_{eff} of dried $Ca(HCO_3)_2$ and annealed $CaCO_3$ particles. Moreover, volume additivity (ideality) is intrinsically assumed in the κ approach. Assuming the value of $\kappa_{GFCO3} = 0.0016$ is applicable to $CaCO_3$, we obtained $\kappa_{HCO3} = 0.030$ from Eq. (8). If we apply $\kappa_{CO_3} = 0.0011 \pm 0.0004$ reported by Sullivan et al. (2009b), we yield only a little larger $\kappa_{HCO3} = 0.031$. However, $\kappa_{HCO3} = 0.03$ is probably only a lower limit, since our experiments in the dry Large Aerosol Chamber indicated the preferential formation of $CaCO_3$(s) in the outer layer of the particles (see below).

3.5 CCN activity of aerosol

We determined the dry diameter of those particles which are activated at a given supersaturation (SS) with a CCN counter. We will call this the critical dry diameter (D_{crit}) which is different from another often used definition of D_{crit} as diameter of the droplet at the maximum of the Köhler curve. The measured D_{crit} are shown in Table 4 and in Fig. 9. $CaCO_3$ particles (red filled squares) activated at significantly larger diameters than the $Ca(HCO_3)_2$(s) particles (blue dots) and the $CaCO_3/Ca(HCO_3)_2$(s) mixed particles (green dots).

The D_{crit} of our spray-dried-annealed $CaCO_3$ agreed well with observations of Sullivan et al. (2009b), who measured $CaCO_3$ aerosol generated by dispersing dry powder (open red squares). The red solid line represents one parameter Köhler calculations with the average κ_{CNNCO3} of 0.0019 ± 0.0007 for $CaCO_3$ from this study. The values of κ_{GFCO3} and κ_{CNNCO3} determined by GF and CCN measurements

agree well within the error limits. Sullivan et al. (2009b) determined the corresponding average $\kappa_{CO_3} = 0.0011 \pm 0.0004$ (red dotted line). The results of our study feature systematically larger κ_{CO_3}, thus somewhat easier droplet activation. However, the average values of both studies agree within the error limits. The red dashed line in Fig. 9 represents the average κ_{CO_3} based on the combination of results of this study and of Sullivan et al. (2009b).

Wet generated water-insoluble or mineral particles often exhibit a severely enhanced hygroscopicity and cloud droplet activation compared to dry generated particles (Herich et al., 2009; Koehler et al., 2007, 2009; Sullivan et al., 2010), which was suggested to be due to the soluble materials on mineral particles introduced by atomizing aqueous suspensions. Impurities also have been suggested to be one explanation for inconsistencies among CCN measurements for adipic acid aerosols generated by atomization of aqueous solutions (Hings et al., 2008). Sullivan et al. (2010) reported a κ of 0.1 for wet-dispersed $CaCO_3$ compared to $\kappa_{CO_3} = 0.0011$ of dry-dispersed $CaCO_3$ aerosols. Considering this huge difference of a factor of 100 in κ, the small difference within the errors between the $CaCO_3$ aerosol generated by our method and the dry-dispersed method of Sullivan is negligible. Both results agree very well, although trace amounts of impurities may also be present in this study, either from the solution or imported with the mineral particle that is concentrated when the droplets dry. This indicates that impurity interference is not important in this study. Moreover, the impurity content in the particles was estimated roughly. To prepare the $Ca(HCO_3)_2$ solutions, 2 g of $CaCO_3$ with a purity of $\geq$99% were added to 1 L of Milli-Q-water (total organic carbon $<$5 ppb, total ion concentration $<$0.05 ppb), i.e. the maximum impurity in the solution is 0.002%. The number mean droplet diameter of the atomizer specified by the manufacturer is 350 nm for water, and the mean particle diameter after drying is 120 nm, therefore the concentrating factor is $\sim$25. If the same density is assumed for the impurity and $CaCO_3/Ca(HCO_3)_2$, it would account for a maximum of 0.05% of the particle mass. Therefore, we conclude that our $CaCO_3$ aerosol is of sufficient quality as required by hygroscopicity and CCN studies.

To our best knowledge there are no studies of the CCN activation of $Ca(HCO_3)_2$ as it was always thought to be too unstable under ambient atmospheric conditions. We are confident that we delivered pure $Ca(HCO_3)_2$(s) particles (non-conditioned, nc) and $CaCO_3/Ca(HCO_3)_2$(s) particles (pre-conditioned, pc) to the CCN spectrometer. The pre-conditioning leading to the $CaCO_3/Ca(HCO_3)_2$(s) mixed salt did not cause large effects on the CCN activity at SS $>$ 0.25% (compare blue and green dots in Fig. 9). Obviously, the presence of 33% $Ca(HCO_3)_2$(s) in the mixed particles was sufficient to cause onset of CCN activation at almost the same critical parameters as in the pure $Ca(HCO_3)_2$(s) particles. The blue and the green solid lines are Köhler calculations with $\kappa_{CCNpc} = 0.14$ and $\kappa_{CCNnc} = 0.16$. With exception of one point at the lowest SS all data points fall on both κ-lines within their errors. In any case dried $Ca(HCO_3)_2$(s) and mixed $CaCO_3/Ca(HCO_3)_2$(s) particles were a factor of 60–70 better CCN than $CaCO_3$ particles.

Both, $\kappa_{CCNpc} = 0.14$ and $\kappa_{CCNnc} = 0.16$ are much larger than the corresponding κ_{GFpc} and κ_{GFnc} of 0.011 and 0.08. This can be explained by the limited solubility of $Ca(HCO_3)_2$ described in the literature. The solubility of $CaCO_3$ is $\approx$0.015 g/l = $1.5 \cdot 10^{-4}$ mol/l in a CO_2 free atmosphere at 25° (Gmelin 1961, p. 933). Raising the CO_2 pressure up to 1 bar (e.g. by bubbling CO_2 to $CaCO_3$ slurry) increases the solubility by a factor of 50 to about 0.008 mol/l (Gmelin 1961, p. 933). The additionally dissolved $CaCO_3$ with increasing CO_2 pressure exists as HCO_3^- in the solutions (Gmelin 1961, p. 927). We approximate the saturation concentration of $Ca(HCO_3)_2$ by about 0.01 mol/l at room temperature and the according saturation mole fraction by 0.01/(0.01+55.5) $\approx$0.0002. The corresponding saturation ratio for an ideal solution would be 0.9998. We thus estimate a deliquescence humidity of $Ca(HCO_3)_2$ around 99% RH. This estimate is reconcilable with our observations of minimal hygroscopic growth for the mixed salt below 92%RH and the absence of deliquescence below 97.5%RH (Fig. 8, green squares). $Ca(HCO_3)_2$ appears to be a non-hygroscopic salt below 97.5%RH, because of its high deliquescence point, but a good CCN because of its still notable solubility.

$Ca(HCO_3)_2$ is somewhat less CCN active than $Ca(NO_3)_2$ (black open squared symbols in Fig. 9, taken from Sullivan et al., 2009b), but it is a better CN than natural mineral dust samples. This is shown in Fig. 9 where the shaded area comprises the range of expectation for CCN activation of atmospheric mineral dust and the black dashed line the median κ of 0.03 suggested by Koehler et al. (2009). In addition κ is given for Arizona Test Dust ($\kappa = 0.025$, blue dashed line) and Saharian Dust ($\kappa = 0.054$, brown dashed line) (Koehler et al., 2009).

$Ca(HCO_3)_2$ is the expected product of the reaction of $CaCO_3$ with CO_2 and H_2O, which have high concentrations in the atmosphere. Thus, especially in cloud droplets of activated mineral dust some $Ca(HCO_3)_2$ may be formed. Several studies on the water soluble inorganic ions in aerosols conducted during ACE-Asia have suggested the co-existence of Ca and carbonate/bicarbonate based on the high correlation between Ca^{2+} and the difference of total cations and anions (Maxwell-Meier et al., 2004; Song et al., 2005). Unfortunately, carbonate and bicarbonate were not measured and could not be differentiated in the particle-into-liquid sampler coupled to a dual-channel ion chromatograph (PILS-IC). The significant enhancement of CCN activity going from $CaCO_3$ to $Ca(HCO_3)_2$ indicates that $CaCO_3$ could become much more CCN active by natural processes especially in remote area when the heterogeneous reactions with pollutant trace gases are negligible.

Table 5. Overview of the experiments in the Large Aerosol Chamber.

Type	Duration	RH	Air supply	CO_2	NO_Y	Final κ_{CCN}
Dry_1	35 h	< 5%	Synth. 6.0	no	1 ppb HNO_3	0.07
Dry_2	23 h	< 5%	Synth. 6.0	no	1 ppb HNO_3	0.1
Humid_1	19 h	40%	Jülich ambient	yes	1 ppb HNO_3	0.45
Humid_2	23 h	40%	Synth. 6.0	no	370 ppb NO, 100 ppb NO_2 370 ppb O_3	0.45

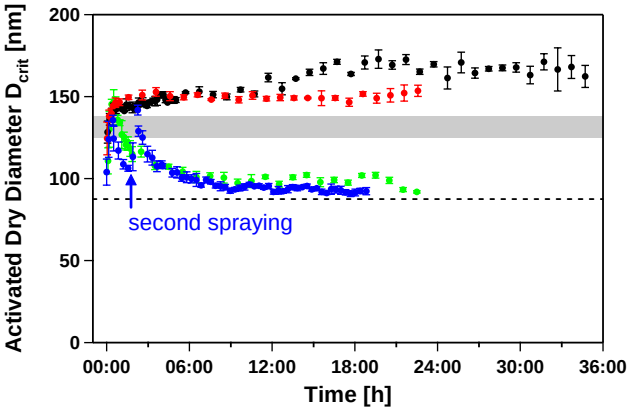

Fig. 10. Time series of activated dry diameters (D_{crit}) of calcium carbonate aerosols at 0.2% SS measured in the Large Aerosol Chamber filled with dry synthetic air (two experiments: red and black), with particle free outside air (containing CO_2(g)) at ~40% RH (blue) and synthetic air at RH ~40% and 470 ppb NO_x (green), dashed line: $D_{crit}(Ca(NO_3)_2)$ by Sullivan et al. (2009b), grey area: D_{crit} ($Ca(HCO_3)_2$ from this study. Error bars are the standard deviation of each measurement interval.

3.6 Long term experiments in the Large Jülich Aerosol Chamber

$Ca(HCO_3)_2$(aq) was introduced into the Large Aerosol Chamber and kept there for up to 36 h. CCN activation, hygroscopic growth factors, and chemical composition by Q-AMS were monitored to capture the long time evolution of the carbonate aerosols under dry and humid conditions. Table 5 provides an overview of the experimental conditions.

The critical diameters D_{crit} at 0.2% SS of the carbonate particles are shown in Fig. 10. In the two dry experiments D_{crit} at 0.2% SS was 127 nm ($\kappa \approx 0.17$) directly after generating the $Ca(HCO_3)_2$ aerosol, which is about the expected value of $\kappa \approx 0.15$ for $Ca(HCO_3)_2$(s) and $CaCO_3/Ca(HCO_3)_2$(s) according to our laboratory scale study above. Thus we assume that we formed some $Ca(HCO_3)_2$(s). During the first 3.5 h the activation diameter increased to 150 nm at 0.2% SS ($\kappa \approx 0.1$) and stayed constant thereafter for the next 5 h. The results of the two experiments differ in that the red curve approaches the final value of 150 nm at 0.2% SS within 2 h and stays constant thereafter, whereas the black curve took somewhat longer to reach the same value. After 10 h the black curve started to rise again and reached values of 170 nm at 0.2% SS ($\kappa \approx 0.07$) within 6 h. We have no explanation for this different behavior, which is not related to changes of RH or T in the chamber. However, we can state that after 22 h/36 h the hygroscopicity parameters κ of 0.1/0.07 were smaller than $\kappa \approx 0.15$ observed for the mixed $CaCO_3/Ca(HCO_3)_2$(s) from the laboratory study. Still, the chamber particles were much better CCN than pure $CaCO_3$ particles with $\kappa = 0.0019 \pm 0.0007$.

Since the tendency for droplet activation was lower than that of the mixed $CaCO_3/Ca(HCO_3)_2$(s) one would expect that the hygroscopic growth was also smaller. However, as is shown in Fig. 11 the aerosol from the chamber (blue triangles, black rhombs, and turquoise triangles) had significantly higher GF than the mixed $CaCO_3/Ca(HCO_3)_2$(s) after preconditioning (green dots). Still, at 95% RH the GF is only 1.165 which translates into $\kappa = 0.18$.

The Q-AMS data showed that the aerosol in the dry chamber after 14 h contained ~40% $Ca(HCO_3)_2$, whereas the mixed $CaCO_3/Ca(HCO_3)_2$(s) aerosol after pre-conditioning contained only 33% bicarbonate. We detected some nitrate uptake of background HNO_3, which was initially about 2% of the CO_2^+ mass and increased slowly to about 4% of the CO_2^+ within 14 h. Therefore, besides residual $Ca(HCO_3)_2$, also $Ca(NO_3)$ must have contributed to the GF and the CCN activity of the particles after 14 h.

These observations can be rationalized by the following considerations. Upon spraying the $Ca(HCO_3)_2$ solution and drying it by mixing with the dry air in the chamber primarily $Ca(HCO_3)_2$(s) aerosol was formed. Favored by the low RH and CO_2 free synthetic air in the chamber the particles lost water and CO_2 over several hours and were slowly converted to the thermodynamically stable $CaCO_3$. However, even after 36 h the particles were much better CCN (κ of 0.1 or 0.07, respectively) than $CaCO_3$ ($\kappa = 0.0019 \pm 0.0007$). Therefore a large portion of $Ca(HCO_3)_2$ was still left in the particles. This is supported by Q-AMS data that showed that after 14 h the $Ca(HCO_3)_2$ accounted still for ~40% of the total calcium salt. Very little gas-phase HNO_3 (2%) was taken up

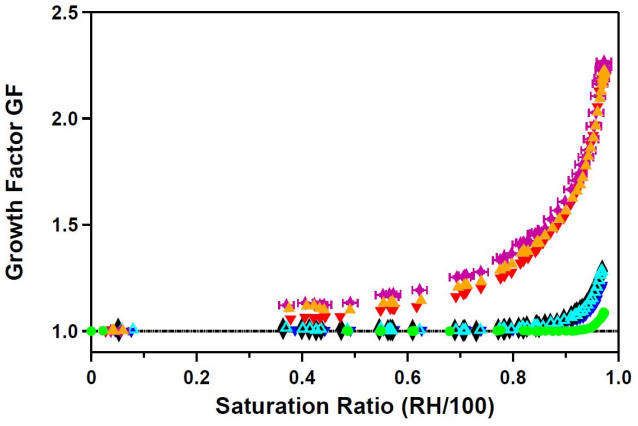

Fig. 11. Humidograms of calcium carbonate aerosols size selected at an electromobility diameter of 150 nm measured in the dry Large Aerosol Chamber (blue: after 1 h, black rhomb: after 16 h, turquoise open triangles: after 20 h). The same in the humidified chamber at 40%RH with 470 ppb NO_x and 370 ppb O_3 added (red triangles: after 3 h, magenta rhombs: after 18 h, orange triangles: after 20 h). In case of the measurements after 20 h the aerosol was additionally dried before entering the HTDMA. For comparison the humidogram of calcium carbonate aerosol *pre-conditioned with water* from the laboratory study (green dots) is shown. Measurement errors: saturation ratio 0.014, GF 0.005 (shown exemplary for one data set).

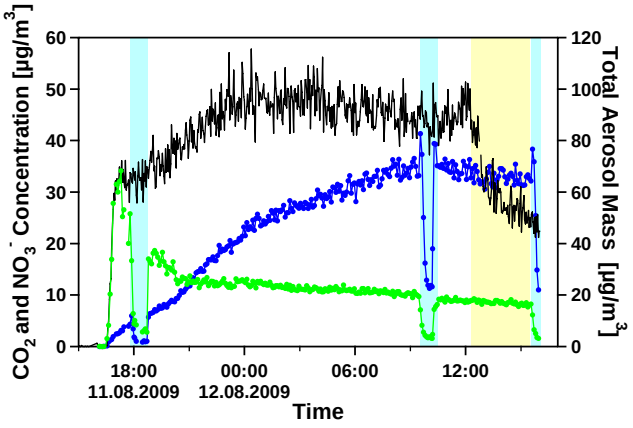

Fig. 12. Experiment in the humidified Large Aerosol Chamber with 470 ppb NO_x added. Time series of CO_2 (green, left axis), NO_3^- (blue, left axis) mass concentrations measured at 900 °C Q-AMS vaporizer temperature and total aerosol mass concentration (black, right axis) calculated from SMPS volume assuming a density of 1.8 g cm^{-3}. Light blue areas: AMS vaporizer at 300 °C. Yellow area: the aerosol was dried with a silica gel diffusion drier before entering the Q-AMS.

instantaneously by the fresh aerosols. Due to the low HNO_3 background and the residual 5% RH, we exclude the formation of significant amounts of surface adsorbed carbonic acid as observed by Al-Hosney and Grassian (2004) at much larger HNO_3 partial pressures. Thereafter nitrate increased only slowly in the dry experiments and had obviously no or small influence since the D_{crit} *increased* with time. We suggest that the surface of the particles reacted quickly according to (Reaction R2), protecting the core of the particles from further conversion. Thus after the relatively fast initial rise the activation diameter increased only slowly. Such a surface to bulk kinetic constrain was suggested before by Vlasenko et al. (2009) for the reaction of nitric acid dust with Arizona Test Dust. Overall $Ca(HCO_3)_2$(s) existed much longer under dry conditions and at room temperature than commonly expected from its thermodynamic stability. Based on the significant difference in CCN activity between $Ca(HCO_3)_2$(s) and $CaCO_3$(s), a longer existence of $Ca(HCO_3)_2$(s) could have important implications for the influence of mineral aerosol on climate.

In the humid chamber (flushed with particle free outside air) D_{crit} at 0.2% SS reached 135 nm ($\kappa = 0.14$) within the first 15 min (blue curve in Fig. 10) which agreed well with $Ca(HCO_3)_2$(s) from our laboratory study (see above). Thereafter we observed a fast decrease of D_{crit}. A second addition of fresh aerosols induced the same behavior. After 20 h activation diameters of 92(±3) nm at 0.2% SS ($\kappa = 0.45$) were reached which were only slightly higher than the 87.5(±3) nm for pure $Ca(NO_3)_2$ ($\kappa = 0.5$) according to Sullivan et al. (2009b) (black dashed line in Fig. 10).

In the second humid experiment NO, NO_2 and O_3 were added on purpose to the aerosols. In this mixture HNO_3 was formed by heterogeneous reaction of NO_2 and N_2O_5 on the particle surfaces and on the chamber walls. The alkaline $Ca(HCO_3)_2$ then obviously reacted with NO_2 and HNO_3 to $Ca(NO_3)_2$. D_{crit} showed the same fast decay and approached the $Ca(NO_3)_2$ values as described above (green curve in Fig. 10).

Also the GF at 90% RH increased rapidly with time and then levelled off (Table 6). The water uptake represented as growth curves (Fig. 11, red and orange) was significantly lower than the water uptake measured for pure $Ca(NO_3)_2$ by Gibson et al. (2006), who find a GF already of 1.77 at 85% RH.

In both humid experiments increasing nitrate was detected at $m/z = 30$ and $m/z = 46$ by the Q-AMS, which replaced HCO_3^-. This is demonstrated in Fig. 12 for the experiment with NO, NO_2, and O_3 addition. However, even after 23 h, still nominal 6% (mole) $Ca(HCO_3)_2$ and 30% $CaCO_3$ can be detected by switching the vaporizer temperature of the AMS between 900°C and 300°C. Together the carbonate (including bicarbonate) contributed about ∼36% of total calcium salt. $Ca(NO_3)_2$ was determined to account for ∼64% (molar content) of the total calcium salt. The total volume of the aerosol increased during the first seven hours. Nitrate and water uptake over-compensated the decrease of aerosol volume concentration due to losses to the chamber walls (Fig. 12).

Table 6. Growth factors at 90% RH, experiment Humid_2.

Time after experiment start	GF(90%)
30 min	1.100
60 min	1.226
4.5 h	1.560
19.5 h	1.609

These observations demonstrated that a substantial heterogeneous conversion into the more soluble $Ca(NO_3)_2$ occurred. We suggest that in early stages of the experiment this took only place on the surface of the particles. But since the nitrate is much more hygroscopic and much better soluble than both, carbonate and bicarbonate, the particles took up water forming a concentrated solution on the surface (Krueger et al., 2003). This further increased the uptake of HNO_3 which is larger on wet particles (Liu et al., 2008a) and also dissolved the upper layers of carbonate. The conversion of $Ca(HCO_3)_2$ to $Ca(NO_3)_2$ thus was accelerated and the reaction of bicarbonate to carbonate was promoted as no protective layer of $CaCO_3$(s) could be formed as suggested for the dry chamber case. Carbonate/bicarbonate decreased as the reaction proceeded but were not completely depleted over the time period of the chamber experiment. Therefore the hygroscopic growth was lower than that of pure nitrate. The $\kappa = 0.45$ for droplet activation of chamber particles at the final stages was only 10% less than that of pure $Ca(NO_3)_2$ as the reaction to nitrate was much faster than that conversion to carbonate.

4 Conclusions

In this study, a novel, easy to operate method was developed using atomization of a $Ca(HCO_3)_2$ solution to produce $CaCO_3$ aerosol, one of the most reactive components in mineral aerosol. In this procedure CO_2 was bubbled through a slurry of $CaCO_3$ dissolving it as bicarbonate. The supernatant solution was decanted, sprayed with an atomizer and dried. Annealing the aerosol in a tube furnace at 300 °C promoted the conversion back to $CaCO_3$.

Q-AMS measurements confirmed that the particles after annealing consisted of pure $CaCO_3$. By hygroscopic growth measurements we derived a hygroscopicity parameter κ(97%RH) of 0.0016 ± 0.0004 for the $CaCO_3$ particles, which agreed with the κ of 0.0019 ± 0.0007 obtained by measurements of CCN activation. The κ from both methods agree very well within the errors and with the κ of 0.0011 ± 0.0004 reported by Sullivan et al. (2009b) for dry-dispersed $CaCO_3$ powder. The new method is suited to generate $CaCO_3$ aerosol of sufficiently high concentration and proper size for studies of hygroscopicity, CCN activity and aerosol chemistry studies in simulation chambers.

Q-AMS measurements further confirmed that the particles obtained by spraying $Ca(HCO_3)_2$ solutions and drying the aerosol to RH<5% consisted of pure $Ca(HCO_3)_2$. This finding could be highly interesting as we have indication that these particles were solid, although $Ca(HCO_3)_2$(s) is thermodynamically unstable under ambient conditions. TEM showed that the $Ca(HCO_3)_2$ particles were solid and spherical like the $CaCO_3$ particles, with $Ca(HCO_3)_2$(s) particles having some internal structures, bubbles or hollow pits. Since in the Q-AMS study pure $Ca(HCO_3)_2$ was observed without excess water, we can rule out inclusions of $Ca(HCO_3)_2$ solution or the formation of metastable hydrates. In addition, in HTDMA measurements $Ca(HCO_3)_2$(s) featured restructuring at 71% RH, which should not be observed in case of liquid particles. Processing the $Ca(HCO_3)_2$(s) particles at 100% RH and drying it again to <5% RH produced mixed $CaCO_3)_2$/$Ca(HCO_3)_2$(s) particles. These mixed particles must have been solid too, since they did not show noticeable hygroscopic growth below 92% RH and GF at 95% was only 1.03. The mixed particles and pure $Ca(HCO_3)_2$(s) were much better CCN ($\kappa = 0.15 \pm 0.02$) than pure $CaCO_3$ ($\kappa = 0.0019 \pm 0.0007$). The difference in CCN activation and hygroscopic growth can be deduced to the limited solubility of $Ca(HCO_3)_2$(s) and a deliquescence point larger than 97.5% RH, which was not assessable by our HTDMA. We therefore hypothesize that we have observed a new, solid phase of $Ca(HCO_3)_2$(s). This must have been a metastable phase and the formation of $CaCO_3$ according the back Reaction (R1) may be hindered when water of the solution evaporates rapidly in the diffusion dryer.

In the dry Large Aerosol Chamber $Ca(HCO_3)_2$(s) was converted over hours to a mixed salt containing ≈40% $Ca(HCO_3)_2$(s) and ≈60% $CaCO_3$. The uptake of HNO_3 was slow, probably due to a similar kinetic hindrance suggested before on the solid Arizona Test Dust particles (Vlasenko et al., 2009). In the dry chamber $Ca(HCO_3)_2$(s) could probably only persist, because it was protected by a $CaCO_3$ coating. $Ca(HCO_3)_2$(s) was shorter lived at 40% RH in ambient Jülich air in the presence of HNO_3 (≈1 ppb) as well as in synthetic air in presence of several hundred ppb NO_x and O_3. In the latter case, carbonate contributed still about ∼36% (including 6% bicarbonate) after about one day and nitrate accounted for ∼64% (molar content) of the total calcium salt.

The chamber experiments showed that $Ca(HCO_3)_2$ can exist longer under atmospheric conditions than conventionally expected from its thermodynamic stability, especially under dry conditions. In the atmosphere $Ca(HCO_3)_2$ can be formed through the reaction of $CaCO_3$ with CO_2 and H_2O, in particular in cloud droplets of activated mineral. A significant increase of CCN activity in going from $CaCO_3$ to $Ca(HCO_3)_2$ by natural processes may alter the role of mineral aerosols in cloud formation, therefore eventually modifying the impact of mineral aerosol on global climate, especially in remote

areas where competing heterogeneous reactions with pollutant trace gases are missing. $Ca(HCO_3)_2$ may be present in the atmosphere for longer times, and likely is faster converted into water soluble salts (e.g. nitrates) than $CaCO_3$.

Acknowledgements. The authors thank the support of the Junior Scientist Exchange Program between the China Scholarship Council and the Helmholtz Association of German Research Centers. We thank both reviewers for the constructive comments which helped to improve the manuscript.

Edited by: M. Ammann

References

Al-Hosney, H. A. and Grassian, V. H.: Carbonic acid: An important intermediate in the surface chemistry of calcium carbonate, J. Am. Chem. Soc., 126, 8068–8069, doi:10.1021/ja0490774, 2004.

Allan, J. D., Delia, A. E., Coe, H., Bower, K. N., Alfarra, M. R., Jimenez, J. L., Middlebrook, A. M., Drewnick, F., Onasch, T. B., Canagaratna, M. R., Jayne, J. T., and Worsnop, D. R.: A generalised method for the extraction of chemically resolved mass spectra from aerodyne aerosol mass spectrometer data, J. Aerosol Sci., 35, 909–922, 2004.

Brecevic, L. and Kralj, D.: On calcium carbonates: from fundamental research to application, Croat. Chem. Acta, 80, 467–484, 2007.

Buchholz, A.: Entwicklung eines Geräts zur Untersuchung des hygroskopischen Wachstums von organischen Aerosolen, Diploma Thesis, Department of Chemistry, University of Cologne, Cologne, 2007.

Claquin, T., Schulz, M., and Balkanski, Y. J.: Modeling the mineralogy of atmospheric dust sources, J. Geophys. Res., 104, 22243–22256, 1999.

DeCarlo, P. F., Slowik, J. G., Worsnop, D. R., Davidovits, P., and Jimenez, J. L.: Particle morphology and density characterization by combined mobility and aerodynamic diameter measurements. Part 1: Theory, Aerosol Sci. Technol., 38, 1185–1205, 2004.

Dinar, E., Mentel, T. F., and Rudich, Y.: The density of humic acids and humic like substances (HULIS) from fresh and aged wood burning and pollution aerosol particles, Atmos. Chem. Phys., 6, 5213–5224, doi:10.5194/acp-6-5213-2006, 2006.

Fairchild, I. J., Smith, C. L., Baker, A., Fuller, L., Spotl, C., Mattey, D., and McDermott, F.: Modification and preservation of environmental signals in speleothems, Earth-Science Rev., 75, 105–153, 2006.

Gibson, E. R., Hudson, P. K., and Grassian, V. H.: Physicochemical properties of nitrate aerosols: Implications for the atmosphere, J. Phys. Chem. A, 110, 11785–11799, 2006.

Gibson, E. R., Gierlus, K. M., Hudson, P. K., and Grassian, V. H.: Generation of internally mixed insoluble and soluble aerosol particles to investigate the impact of atmospheric aging and heterogeneous processing on the CCN activity of mineral dust aerosol, Aerosol Sci. Technol., 41, 914–924, 2007.

Gmelin: Das System $CaO - CO_2 - H_2O$, Gmelins Handbuch der anorganischen Chemie 8, System Nummer 28, Calcium, Teil B, Weinheim, Verlag Chemie, 928–935, 1961.

Herich, H., Tritscher, T., Wiacek, A., Gysel, M., Weingartner, E., Lohmann, U., Baltensperger, U., and Cziczo, D. J.: Water uptake of clay and desert dust aerosol particles at sub- and supersaturated water vapor conditions, Phys. Chem. Chem. Phys., 11, 7804–7809, doi:10.1039/b901585j, 2009.

Hings, S. S., Wrobel, W. C., Cross, E. S., Worsnop, D. R., Davidovits, P., and Onasch, T. B.: CCN activation experiments with adipic acid: effect of particle phase and adipic acid coatings on soluble and insoluble particles, Atmos. Chem. Phys., 8, 3735–3748, doi:10.5194/acp-8-3735-2008, 2008.

House, W. A.: Kinetics of crystallization of calcite from calcium bicarboante solutions, J. Chem. Soc. Farad. Trans. I, 77, 341–359, 1981.

Jayne, J. T., Leard, D. C., Zhang, X. F., Davidovits, P., Smith, K. A., Kolb, C. E., and Worsnop, D. R.: Development of an aerosol mass spectrometer for size and composition analysis of submicron particles, Aerosol Sci. Technol., 33, 49–70, 2000.

Jonas, P. R., Charlson, R. J., and Rodle, H.: Climate change 1994: radiation of Climate Change and An Evaluation of the Changes, Cambridge University Press, Cambridge, 1995.

Keiser, E. H. and Leavitt, S.: On the preparation and the composition of the acid carbonates of calcium and barium, J. Am. Chem. Soc., 30, 1711–1714, 1908.

Koehler, K. A., Kreidenweis, S. M., DeMott, P. J., Prenni, A. J., and Petters, M. D.: Potential impact of Owens (dry) Lake dust on warm and cold cloud formation, J. Geophys. Res., 112, D12210, doi:10.1029/2007jd008413, 2007.

Koehler, K. A., Kreidenweis, S. M., DeMott, P. J., Petters, M. D., Prenni, A. J., and Carrico, C. M.: Hygroscopicity and cloud droplet activation of mineral dust aerosol, Geophys. Res. Lett., 36, L08805, doi:10.1029/2009gl037348, 2009.

Krueger, B. J., Grassian, V. H., Laskin, A., and Cowin, J. P.: The transformation of solid atmospheric particles into liquid droplets through heterogeneous chemistry: laboratory insights into the processing of calcium containing mineral dust aerosol in the troposphere, Geophys. Res. Lett., 30(4), L1148, doi:10.1029/2002GL016563, 2003.

Laskin, A., Iedema, M. J., Ichkovich, A., Graber, E. R., Taraniuk, I., and Rudich, Y.: Direct observation of completely processed calcium carbonate dust particles, Farad. Discuss., 130, 453–468, 2005.

Liu, Y., Gibson, E. R., Cain, J. P., Wang, H., Grassian, V. H., and Laskin, A.: Kinetics of heterogeneous reaction of CaCO3 particles with gaseous HNO_3 over a wide range of humidity, J. Phys. Chem. A, 112, 1561–1571, 2008a.

Liu, Y. J., Zhu, T., Zhao, D. F., and Zhang, Z. F.: Investigation of the hygroscopic properties of $Ca(NO_3)_2$ and internally mixed $Ca(NO_3)_2/CaCO_3$ particles by micro-Raman spectrometry, Atmos. Chem. Phys., 8, 7205–7215, doi:10.5194/acp-8-7205-2008, 2008b.

Marquardt, A., Hackfort, H., Borchardt, J., Schober, T., and Friedrich, J.: TEM-Untersuchungen der Mikrostrukturen von Verbrennungsaerosolen, Berichte des Forschungszentrums Jülich; JUEL-2700, ISSN 0366-0885, 1992.

Matthew, B. M., Middlebrook, A. M., and Onasch, T. B.: Collection efficiencies in an Aerodyne Aerosol Mass Spectrometer as a function of particle phase for laboratory generated aerosols, Aerosol Sci. Technol., 42, 884–898, doi:10.1080/02786820802356797, 2008.

Maxwell-Meier, K., Weber, R., Song, C., Orsini, D., Ma, Y., Carmichael, G. R., and Streets, D. G.: Inorganic composition of fine particles in mixed mineral dust-pollution plumes observed from airborne measurements during ACE-Asia, J. Geophys. Res.-Atmos., 109(20) D19s07, doi:10.1029/2003jd004464, 2004.

Mensah, A. A., Buchholz, A., Mentel, Th. F., Tillmann, R., and Kiendler-Scharr, A.: Determination of the relative ionization efficiency of water in an Aerodyne aerosol mass spectrometer, J. Aerosol Sci., in review, 2010.

Mentel, T. F., Bleilebens, D., and Wahner, A.: A study of nighttime nitrogen oxide oxidation in a large reaction chamber – The fate of NO_2 N_2O_5, HNO_3, and O_3 at different humidities, Atmos. Environ., 30, 4007–4020, 1996.

Miller, J. P.: A portion of the system calcium carbonate-carbon dioxide-water, with geological implications, Am. J. Sci., 250, 161–203, 1952.

Murray, J. W.: The deposition of Calcite and Aragonite in caves, J. Geol., 62, 481–492, 1954.

Okada, K., Qin, Y., and Kai, K.: Elemental composition and mixing properties of atmospheric mineral particles collected in Hohhot, China, Atmos. Res., 73, 45–67, 2005.

Petters, M. D. and Kreidenweis, S. M.: A single parameter representation of hygroscopic growth and cloud condensation nucleus activity, Atmos. Chem. Phys., 7, 1961–1971, doi:10.5194/acp-7-1961-2007, 2007.

Prince, A. P., Grassian, V. H., Kleiber, P., and Young, M. A.: Heterogeneous conversion of calcite aerosol by nitric acid, Phys. Chem. Chem. Phys., 9, 622–634, 2007.

Sanders, J. P. and Gallagher, P. K.: Kinetic analyses using simultaneous TG/DSC measurements Part I: decomposition of calcium carbonate in argon, Thermochim. Acta, 388, 115–128, 2002.

Santschi, C. and Rossi, M. J.: Uptake of CO_2, SO_2, HNO_2 and HCl on calcite (CaCO3) at 300 K: Mechanism and the role of adsorbed water, J. Phys. Chem. A, 110, 6789-6802, doi:10.1021/jp056312b, 2006.

Song, C. H., Maxwell-Meier, K., Weber, R. J., Kapustin, V., and Clarke, A.: Dust composition and mixing state inferred from airborne composition measurements during ACE-Asia C130 Flight #6, Atmos. Environ., 39, 359–369, 2005.

Sullivan, R. C., Guazzotti, S. A., Sodeman, D. A., and Prather, K. A.: Direct observations of the atmospheric processing of Asian mineral dust, Atmos. Chem. Phys., 7, 1213–1236, doi:10.5194/acp-7-1213-2007, 2007.

Sullivan, R. C., Moore, M. J. K., Petters, M. D., Kreidenweis, S. M., Roberts, G. C., and Prather, K. A.: Timescale for hygroscopic conversion of calcite mineral particles through heterogeneous reaction with nitric acid, Phys. Chem. Chem. Phys., 11, 7826–7837, 2009a.

Sullivan, R. C., Moore, M. J. K., Petters, M. D., Kreidenweis, S. M., Roberts, G. C., and Prather, K. A.: Effect of chemical mixing state on the hygroscopicity and cloud nucleation properties of calcium mineral dust particles, Atmos. Chem. Phys., 9, 3303–3316, doi:10.5194/acp-9-3303-2009, 2009b.

Sullivan, R. C., Moore, M. J. K., Petters, M. D., Kreidenweis, S. M., Qafoku, O., Laskin, A., Roberts, G. C., and Prather, K. A.: Impact of particle generation method on the apparent hygroscopicity of insoluble mineral particles, Aerosol Sci. Technol., 44, 830–846, 2010.

Usher, C. R., Michel, A. E., and Grassian, V. H.: Reactions on mineral dust, Chem. Rev., 103, 4883–4939, 2003.

Vlasenko, A., Sjogren, S., Weingartner, E., Stemmler, K., Gäggeler, H. W., and Ammann, M.: Effect of humidity on nitric acid uptake to mineral dust aerosol particles, Atmos. Chem. Phys., 6, 2147–2160, doi:10.5194/acp-6-2147-2006, 2006.

Vlasenko, A., Huthwelker, T., Gaggeler, H. W., and Ammann, M.: Kinetics of the heterogeneous reaction of nitric acid with mineral dust particles: an aerosol flowtube study, Phys. Chem. Chem. Phys., 11, 7921–7930, 10.1039/b904290n, 2009.

Wahner, A., Mentel, T. F., and Sohn, M.: Gas-phase reaction of N_2O_5 with water vapor: Importance of heterogeneous hydrolysis of N_2O_5 and surface desorption of HNO_3 in a large teflon chamber, Geophys. Res. Lett., 25, 2169–2172, 1998.

Wiedensohler, A.: An approximation of the bipolar charge-distribution for particles in the sub-micron size range, J. Aerosol. Sci., 19, 387–389, 1988.

Zhang, X. Y., Gong, S. L., Shen, Z. X., Mei, F. M., Xi, X. X., Liu, L. C., Zhou, Z. J., Wang, D., Wang, Y. Q., and Cheng, Y.: Characterization of soil dust aerosol in China and its transport and distribution during 2001 ACE-Asia: 1. Network observations, J. Geophys. Res., 108(13), 4621, doi:10.1029/2002jd002632, 2003.